SAND2014-20075C

# Development of a List-Mode Ideal Observer to Perform Classification Tasks when Imaging Nuclear Inspection Objects under Signal-Known-Exactly Conditions

Christopher J. MacGahan, *Student Member, IEEE,* Matthew A. Kupinski, Nathan R. Hilton, William C. Johnson, and Erik M. Brubaker

***Abstract*—We developed a signal-known-exactly version of the ideal observer that processes data in list-mode format to perform binary classification, a useful task for arms-control treaty applications. This observer offers the best possible performance and future observer models developed in our work will be compared to this model. The two examined sources were plutonium inspection objects developed by Idaho National Lab. We modeled a fast-neutron coded-aperture imager, developed by Oak Ridge National Lab and Sandia National Labs to acquire simulation data. Monte Carlo simulations using the GEANT4 toolkit tracked photons and neutrons from these objects to the imager. The observer model was evaluated using the area under the ROC curve for multiple background strengths.**

## I. Introduction

CURRENT nonproliferation-treaty verification methods that use image reconstruction require a hardware or software information barrier to separate the detector operator from these images. Our goal is to develop and study mathematical observer models that perform tasks without reconstructing images or aggregating sensitive information. Ideally, we want these observer models to process data in list-mode format–reading the data recorded in each event, updating a test statistic that will be used to make decisions, and throwing that data away. This is a unique task in that there is generally little incentive to prevent imaging operators from visualizing what they are imaging. However, we believe these methods could also be applicable to airport security imaging. They offer the possibility of imaging people and making decisions on potential security risks without those in control of the detector seeing the sensitive images.

The ideal observer has complete probabilistic knowledge of the image data and offers the best possible performance for a given task [1]. In this paper we formulate the theory for a signal-known-exactly (SKE) version of the ideal observer that performs binary classification using list-mode data. This SKE model serves as the first step toward a more thorough model that accurately describes the physical processes evident in real-world classification tasks. It also serves as upper bound for all future observers that will be generated by this project that store less information than the ideal observer.

Manuscript received November 26, 2014. This work is supported by the Office of Defense Nuclear Nonproliferation Research and Development, Nuclear Weapon and Material Security Team. Sandia National Laboratories is a multi-program laboratory managed and operated by Sandia Corporation, a wholly owned subsidiary of Lockheed Martin Corporation, for the U.S. Department of Energy's National Nuclear Security Administration under contract DE-AC04-94AL85000. (SAND2014-XXXXX)

C. J. MacGahan (e-mail: cmacgahan@optics.arizona.edu) is a Ph.D. candidate and M. A. Kupinski is a professor in the College of Optical Sciences, University of Arizona, Tucson AZ 85721. C. J. MacGahan was partially funded by the Technology Research Initiative Fund (TRIF) imaging fellowship during the 2013-2014 academic year.

N. R. Hilton, W. C. Johnson and E. M. Brubaker are with Sandia National Labs, Livermore, CA 94551

## II. Theory

We start by formalizing the theory for list-mode data, using a similar framework to one developed by Luca Caucci [2]. There are two components to the image data collected. Each detector pixel will be hit by $N$ photons or neutrons and each event contains a set of list-mode parameters $A_n$,

$$A_n = \{\text{particle type, pixel number, energy absorbed}\}. \quad (1)$$

The ideal observer makes decisions by thresholding the ratio of the likelihood of observing the data given the $H_2$ hypothesis (source 2 present) compared to the $H_1$ hypothesis (source 1 present) [1]

$$\Lambda(\{A_n\}, \mathbf{N}) = \frac{pr(\{A_n\}, \mathbf{N}|H_2)}{pr(\{A_n\}, \mathbf{N}|H_1)}. \quad (2)$$

where $\{A_n\}$ is the list-mode data for all detected particles and $\mathbf{N}$ is a vector containing the number of counts in each pixel.

### A. Single pixel case

Under SKE conditions, the background-count rate $\overline{N_b}$ and signal-count rate for source $j$ $\overline{N_j}$ are known for the pixel. Under a set acquisition time, the ideal observer takes the form

$$\Lambda_{SKE}(\{A_n\}, N|\overline{N_b}, \overline{N_1}, \overline{N_2}) = \frac{pr(\{A_n\}, N|\overline{N_b}, \overline{N_2}, H_2)}{pr(\{A_n\}, N|\overline{N_b}, \overline{N_1}, H_1)}. \quad (3)$$

The spectrum and number of counts observed on each pixel are independent. Noting this, we split the likelihoods in (3) into two components,

$$\begin{aligned} pr(\{A_n\}, N|\overline{N_b}, \overline{N_j}, H_j) =& Pr(N|\overline{N_b}, \overline{N_j}, H_j) \\ & \times pr(\{A_n\}|N, \overline{N_b}, \overline{N_j}, H_j) \end{aligned} \quad (4)$$

where $pr$ represents the probability density function of a continuous random variable and $Pr$ the probability of a

discrete random variable. The first term on the right of (4) is a Poisson probability on the number of observed counts given the expected number of detected counts from the background and source. This can be written as a sum over the various combinations of detected signal counts $N_j$ and background counts $N_b$ that sum to $N$ total counts

$$Pr(N|\overline{N_b},\overline{N_j},H_j) = \sum_{N_b=0}^{N_b=N} Pr(N_b|\overline{N_b})Pr(N-N_b|\overline{N_j}). \tag{5}$$

However, a convolution of 2 Poissons with different means results in a Poisson distribution with a mean value equal to the sum of those means

$$Pr(N|\overline{N_b},\overline{N_j},H_j) = Pr(N|(\overline{N_b}+\overline{N_j})). \tag{6}$$

Taking the right side of (4), we recognize each observed event is independent, resulting in

$$pr(\{A_n\}|N,\overline{N_b},\overline{N_j},H_j) = \prod_{n=1}^{N} pr(A_n|\overline{N_b},\overline{N_j},H_j). \tag{7}$$

We now define the spectrum due to source $j$ $h_j$ and spectrum due to the background $h_b$. The probability of detecting a particular list-mode energy is then

$$\begin{aligned} pr(A_n|\overline{N_b},\overline{N_j},H_j) = {} & pr(A_n|h_b)Pr(h_b|\overline{N_b},\overline{N_j})+ \\ & pr(A_n|h_j)Pr(h_j|\overline{N_b},\overline{N_j}). \end{aligned} \tag{8}$$

$pr(A_n|h_j)$ is the background spectral probability of detecting that particle's energy. $Pr(h_b|\overline{N_b},\overline{N_j})$ is the probability that the detected particle is from the background, which is a simple ratio of the background count rate and overall count rate $\frac{\overline{N_b}}{\overline{N_b}+\overline{N_j}}$

$$\begin{aligned} pr(A_n|\overline{N_b},\overline{N_j},H_j) = {} & \frac{\overline{N_b}}{\overline{N_b}+\overline{N_j}} pr(A_n|h_b)+ \\ & \frac{\overline{N_j}}{\overline{N_j}+\overline{N_b}} pr(A_n)|h_j) \\ = {} & \frac{\overline{N_b}pr(A_n|h_b)+\overline{N_j}pr(A_n|h_j)}{\overline{N_j}+\overline{N_b}}. \end{aligned} \tag{9}$$

Substituting (9) and (6) into (4)

$$\begin{aligned} & pr(\{A_n\},N|\overline{N_b},\overline{N_j},H_j) = \\ & Pr(N|\overline{N_b}+\overline{N_j})\frac{\overline{N_b}pr(A_n|h_b)+\overline{N_j}pr(A_n|h_j)}{\overline{N_j}+\overline{N_b}}. \end{aligned} \tag{10}$$

This equation essentially has two components, similar to (4)–a Poisson component on the total number of counts observed, and a spectral probability term given by the mean spectrum found on the detector pixel. We can further define a mean count rate and mean spectral density for the combined background and signal

$$\begin{aligned} pr(A_n|h_{jb}) &= \frac{\overline{N_b}pr(A_n|h_b)+\overline{N_j}pr(A_n|h_j)}{\overline{N_j}+\overline{N_b}} \\ Pr(N|\overline{N_{jb}}) &= Pr(N|\overline{N_b}+\overline{N_j}). \end{aligned} \tag{11}$$

This leads to the final expression for the likelihood,

$$pr(\{A_n\},N|\overline{N_b},\overline{N_j},H_j) = Pr(N|\overline{N_{jb}})\prod_{n=1}^{N} pr(A_n|h_{jb}), \tag{12}$$

and the ideal observer

$$\begin{aligned} & \Lambda_{SKE}(\{A_n\},N|\overline{N_b},\overline{N_1},\overline{N_2}) = \\ & \qquad \frac{Pr(N|\overline{N_{2b}})}{Pr(N|\overline{N_{1b}})}\prod_{n=1}^{N}\frac{pr(A_n|h_{2b})}{pr(A_n|h_{1b})}. \end{aligned} \tag{13}$$

We envision the classification process occurring in two stages. First, in the calibration stage, calibration data is read in from one pair of sources, aggregating data in order to develop the count and spectral parameters used in the observers. $h_{1b}$, $\overline{N_{1b}}$, $h_{2b}$, and $\overline{N_{2b}}$ are set equal to the calibration data. Second, in the testing stage, the test statistic $\Lambda$ for the SKE ideal observer which is thresholded to make decisions is initialized to one. The particle is detected, its energy is observed and $\Lambda$ is multiplied by the ratio of spectral probabilities for that energy under the two hypothesis. That detected particle is then forgotten–its information is only used to update the test statistic. This process continues for all particles recorded in the acquisition time. Finally, $\Lambda$ is multiplied by the ratio of Poisson probabilities for observing $N$ counts in that acquisition time given the two hypothesis. It should be noted that $N$ is not a list-mode value as it requires storing information from one event to the next, but this is a necessary drawback of the ideal observer that we hope to avoid in the development of future observers. $\Lambda$ is then thresholded to make a decision. We believe this model is one possible way of using detector data from an imager while avoiding an information barrier.

### *B. M pixel case*

Discussion in the prior section focused on development of the SKE ideal observer for a single pixel. Taking this analysis to $M$ pixels is simple under the assumption that every pixel is independent. Our detector data becomes the number of counts detected by the $m^{th}$ pixel $N_m$ and the list-mode data of particles hitting that pixel $A_{nm}$. The numerator and denominator in (3) each become a product over the likelihood for each individual pixel, and the same math discussed in (7)-(12) applies with the understanding that each spectrum and mean detected counts are pixel dependent. In the $M$ pixel case, $N$, $\overline{N_b}$, $\overline{N_j}$ all become vectors (denoted in bold below) of length $M$. The SKE ideal observer then becomes

$$\Lambda_{SKE}(\{A_n\},\mathbf{N}|\overline{\mathbf{N}_b},\overline{\mathbf{N}_1},\overline{\mathbf{N}_2}) = \frac{pr(\{A_n\},\mathbf{N}|\overline{\mathbf{N}_b},\overline{\mathbf{N}_2},H_2)}{pr(\{A_n\},\mathbf{N}|\overline{\mathbf{N}_b},\overline{\mathbf{N}_1},H_1)} \tag{14}$$

with the individual likelihoods given by

$$\begin{aligned} & pr(\{A_n\},\mathbf{N}|\overline{\mathbf{N}_b},\overline{\mathbf{N}_j},H_j) = \\ & \qquad \prod_{m=1}^{M} Pr(N_m|\overline{N_{jbm}})\prod_{n=1}^{N_m} pr(A_{nm}|h_{jbm}). \end{aligned} \tag{15}$$

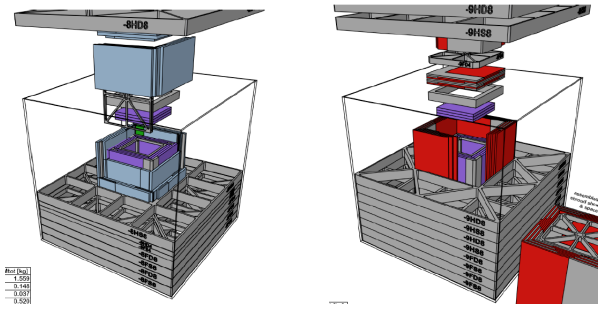

Fig. 1. Inspection objects 8 and 9 developed by INL [5]. Object 8 is plutonium shielded by depleted uranium while object 9 is plutonium shielded by highly-enriched uranium. Both assemblies are supported by an aluminum framework inside an 8" by 8" aluminum box.

Combining (15) with (14),

$$\Lambda_{SKE}(\{A_n\}, \mathbf{N}|\overline{\mathbf{N}_b}, \overline{\mathbf{N}_1}, \overline{\mathbf{N}_2}) = \prod_{m=1}^{M} \frac{Pr(N_m|\overline{N_{2bm}})}{Pr(N_m|\overline{N_{1bm}})} \prod_{n=1}^{N_m} \frac{pr(A_{nm}|h_{2bm})}{pr(A_{nm}|h_{1bm})} \quad (16)$$

Calibration data requires the number of signal and background counts $N_{jbm}$ and spectral density for each pixel. Similar to the single pixel case, the test statistic $\Lambda$ is initialized to one. For each particle read in, its energy is observed and $\Lambda$ is multiplied by the ratio of spectral probabilities specific to its pixel number. When the acquisition time is over, $\Lambda$ is multiplied by the ratio of Poisson probabilities under the two hypothesis for each pixel. This means $\Lambda$ is multiplied by $M$ probability ratios.

## III. Simulation

### A. Objects and Imager

Classification tasks were performed on inspection objects 8 and 9 developed by Idaho National Lab (INL) [5]. Due to significant shielding of gamma rays, multiple variance reduction methods were used to acquire an appreciable amount of data in a reasonable period of time. The most useful step was to choose not to emit any gammas below 100 keV, as there is a peak at 60 keV that is roughly three orders of magnitude more intense than any individual peak above 100 keV. We will expand on this process and verify the object models in a paper we plan to publish in 2015. Snapshots taken from the schematics of these sources are shown in Figure 1.

The detector modeled in these studies is a fast-neutron coded-aperture imager (shown in Figure 2), developed by Oak Ridge National Lab and Sandia National Labs. The system is designed to detect neutrons, but the mask causes attenuation in gamma rays as well.

### B. Forward model in GEANT4

The detector and INL sources were coded into our Monte Carlo transport application that uses the GEANT4 toolkit [3], [4]. The simulation setup is shown in Figure 3. Photons and neutrons were tracked from these objects to the detector. Due to a very low detection probability, photons were emitted with a linear energy bias and an energy cutoff of 100 keV. A detector-response code collects the light output and bins it into a mean pixel location. Perfect pulse-shape discrimination between gammas and neutrons is assumed.

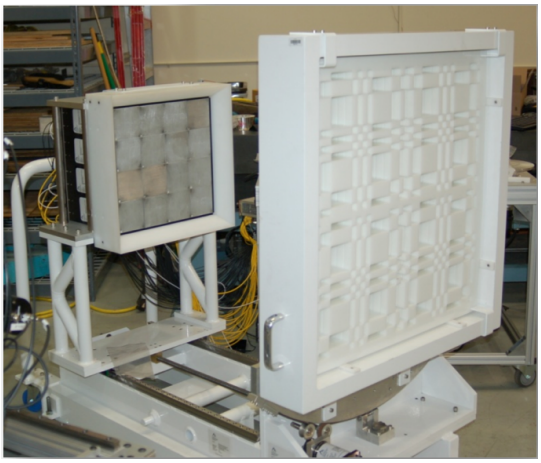

Fig. 2. Fast neutron coded aperture imaging system [6]. The imager uses a polyethylene coded aperture and a 4x4 array of liquid-scintillator detectors, each consisting of 10x10 1cm$^2$ pixels.

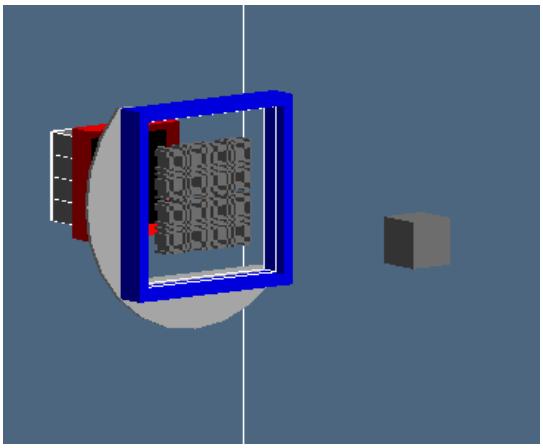

Fig. 3. Geant4 model of system. INL object 8 is stored inside aluminum cube. The grey geometries in the mask are holes, and transparent sections are the Polyethylene material (shown this way for visibility). A quarter inch lead plate (black) is in front of the pixels, blocking low energy gammas.

The two imaged sources have notably different gamma-ray detection rates and energy spectra due to the material choice for the shielding component(see Figure 4). A low number of bins was chosen for the energy spectra in order to improve the SNR of the energy bin data to prevent overly certain observer model results. The simulated data corresponds to about 100s of real-life time. In an actual experiment, the acquisition time could be increased to improve the energy resolution of the two spectra.

### C. Background

The background was generated using the Gamma Detector and Response Software (GADRAS). A plastic scintillator was created that best modeled the known physical properties of

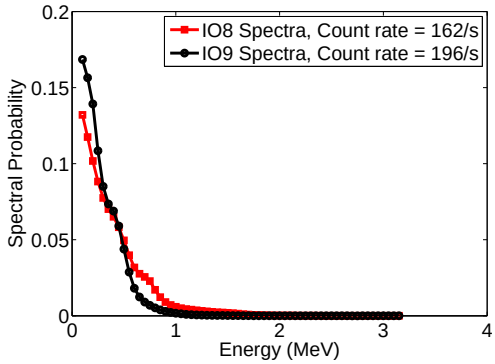


Fig. 4. Comparison of IO8 and IO9 data. IO9 with the more active shielding material HEU and a peak at 185keV shifts the spectrum towards lower energies and increases count rate

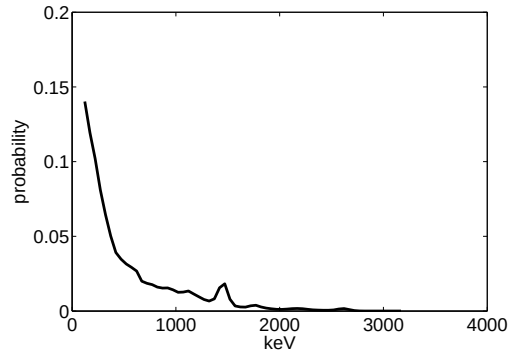


Fig. 5. Background created with 1.21%K40, 1.66 ppm of uranium and 5.54 ppm of thorium were used to create the spectrum. This corresponds to the background in Buffalo, NY.

the liquid scintillator in our detector. Spectral templates were created for cosmic muons, 1.01% K40, 10ppm of thorium and 5ppm of uranium. Using these templates, background spectra can be created for any location. An example gamma-ray background is shown in Figure 5. This background spectrum was added to all pixels.

### *D. Experimental outline*

Two data sets were found for each object under a chosen orientation and location. The first pair is treated as calibration data and used to find the appropriate $H_2$ and $H_1$ parameters in the observer models as discussed above. These observer models are then used to classify sample data taken from the second set.

### *E. Evaluating performance*

Observer models were evaluated using the area under the ROC curve (AUC), computed using the two-alternative forced-choice test [7]. The observer is presented with a series of pairs of datasets. In each pair, one dataset is from a measurement of source 1, and the other is from a measurement of source 2. For each dataset, the observer calculates a test statistic (e.g. $\Lambda$ in (16)) that is intended to have a higher value for source 2 than for source 1. The fraction of pairs in which the test

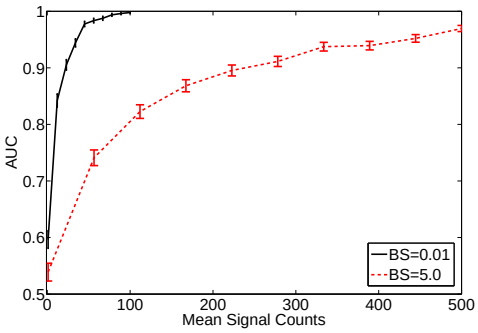


Fig. 6. This plot shows SKE observer performance under weak and strong backgrounds. The SKE observer with a background to signal ratio of 0.01 shows unrealistically good performance (20 signal counts to achieve an AUC of 0.9). When the background to signal ratio is ramped up to 5, about a factor of 10 more signal counts are required.

statistic is higher for the actual source 2 dataset is equivalent to the AUC.

## IV. Results

The following simulation study reflects a real world binary classification task with objects IO8 and IO9 under known orientation and location. The calibration data and testing data were taken from separate simulations. The calibration set was used to develop the observer in (16) and samples were taken from the testing set to study the performance of this model. Observer performance with a weak background and strong background is shown in Figure 6. As expected, performance falls off as the background strength increases.

Performance for this specific task is very strong in the weak background case, as 20 signal counts corresponds to approximately 0.1 seconds of acquisition time. Generally, performance is task-specific, and admittedly an easy task was chosen here as the spectra of these two sources are easy to differentiate. We remind the reader that this study is under a very strict set of circumstances. Data for each pixel was assumed to be independent, the background was assumed to have no spatial variation, electronic noise was ignored and nuisance parameters, such as object orientation, location and material age, were not considered. As other sources of error are included in the model, performance will decrease. However, the takeaway from this result is that the framework developed here can potentially be used to classify inspection objects under an optimal set of circumstances without reconstruction or the storage of sensitive information.

## V. Conclusion

This work describes the implementation of an SKE ideal observer that processes information in list-mode format, updating a single test statistic and avoiding storage of sensitive information when classifying objects. While this is a useful result for nonproliferation treaty purposes, it is ultimately limited– it is very unlikely that the position, orientation and material age of the source materials is exactly known. Development of observer models that take these nuisance parameters into

account is a necessity and our work on this subject will be submitted to a journal in the near future. In addition, the forward model needs to become more physically accurate. Incorrect pulse shape discrimination, more realistic background models, electronic noise and other sources of variability not currently modeled in our simulations must be taken into account. The ideal observer offers optimal performance when all sources of variability are included, but the theory presented here does not completely describe a real world experiment yet. Finally, observer models that store less information than the ideal observer will be studied and their performance will be compared to this best case scenario.

## REFERENCES


[1] H. H. Barrett and K. J. Myers, *Foundations of Image Science*, 1st ed. (Wiley, 2004).

[2] L. Caucci and H.H. Barrett, "Objective assessment of image quality V. Photon-counting detectors and list-mode data", J. Opt. Soc. Am. A **29**(6) pp 1003-1016 (2012).

[3] S. Agostinelli et al, "Geant4 - a simulation toolkit", Nucl. Instrum. Methods Phys. Res. A, **506**(3) pp. 250-303 (2003).

[4] J. Allison et al. "Geant4 Developments and Applications", *IEEE Transactions on Nuclear Science* , **53**(1) pp. 270-278 (2006).

[5] R. Neibert, J. Zabriskie, C. Knight, and J. L. Jones, *Passive and Active Radiation Measurements Capability at the INL Zero Power Physics Reactor (ZPPR) Facility*, Idaho National Laboratory report INL/EXT-11-20876, Idaho Falls, Idaho, December 2010.

[6] P. A. Hausladen, M. A. Blackston, E. Brubaker, D. L. Chichester, P. Marleau, and R. J. Newby, "Fast-neutron coded-aperture imaging of special nuclear material configurations", *Proc. of 53rd INMM Annual Meeting, Orlando*, Florida, 2012.

[7] G. T. Fechner, E. G. Boring, D. H. Howes (Eds.), *Elements of Psychophysics*, Holt, Rinehart and Winston, New York (1966 [1860])